Study On The Cutting Mechanism of Randomly Deflected Truncated Cone Shape Single Abrasive Grain

Lansheng Zhang
Qingdao University of Technology
Jing Liang Jiang (cba1981@126.com)
Qingdao Technological University - Huangdao Campus https://orcid.org/0000-0003-0136-8176
Dexiang Wang
Qingdao University of Technology
Shufeng Sun
Qingdao University of Technology

Research Article

Keywords: Random deflection angle, Single abrasive grain cutting, mechanism Research

Posted Date: October 19th, 2021

DOI: https://doi.org/10.21203/rs.3.rs-973761/v1

Version of Record: A version of this preprint was published at The International Journal of Advanced Manufacturing Technology on February 17th, 2022. See the published version at https://doi.org/10.1007/s00170-022-08824-x.

Study on the cutting mechanism of randomly deflected truncated cone shape single abrasive grain

Lansheng Zhang[1], Jingliang Jiang[1]*, Dexiang Wang[1], Shufeng Sun[1]

[1]School of Mechanical & Automotive Engineering, Qingdao University of Technology, Qingdao 266520, China

* Corresponding author: Jingliang Jiang: E-mail: cba1981@126.com; telephone number: 86+ 18353229686; Address: 777 Jialingjiang East Road, Huangdao District, Qingdao City, Shandong Province, China

First author: Lansheng Zhang E-mail: zlsd163youxiang@163.com; telephone number: 86+ 17806233985; Address: 777 Jialingjiang East Road, Huangdao District, Qingdao City, Shandong Province, China

Abstract: Based on the random distribution characteristic of abrasive grains for the grinding wheel circumference surface during the manufacturing process, considering the grinding parameters and deflection parameters comprehensively, a randomly deflected truncated cone shape single abrasive grain cutting simulation model was established. Then, studying its cutting mechanism: the trajectory length value by numerical method and formula method were compared, the consequence indicates that the error is extremely small, this demonstrates the accuracy of the numerical method. The calculation and analysis of the workpiece cutting surface topography and the undeformed chip shape were carried out, it shows that the cutting surface topography and the undeformed chip shape are coincident. The influence laws of each grinding process parameter on the material removal volume (*MRV*) and material removal rate (*MRR*) were investigated, the results display that the grinding method affects the changing pattern of *MRV* and *MRR*, when the grinding method was up-grinding, a high wheel speed or a small wheel diameter are able to enhance the *MRR*, the *MRV* and *MRR* are increments with the increasing workpiece feed speed or

abrasive grain cutting depth, and the *MRV* and *MRR* decrease with the raising of the absolute value of single abrasive grain deflection angle. The situation is a similar or opposite trend in down grinding. This work can provide a theoretical reference for the selection and optimization of grinding parameters, and further lay a foundation for the research in the grinding mechanism of the grinding wheel.

Keywords: Random deflection angle; Single abrasive grain cutting; mechanism Research

1 Introduction

Precision manufacturing equipment and its related frontier theory research have been a highlight area of concern in recent years, grinding is an important precision and ultra-precision processing method in manufacturing, precision machining grinding process, generally, as the last process of machining, can effectively eliminate the processing defects that generated by the previous process, improve the quality of product processing, and play a very important role in ensuring the performance and service life of the product [1-2]. Grinding technology, as one of the important developments of modern manufacturing technology, is widely used in aerospace, precision instruments, automobiles, and other manufacturing fields [3-6]. The grinding process can be regarded as the comprehensive effect of slipping, plowing, and cutting by a large number of discrete abrasive grains which are distributed on the grinding wheel surface, and is a multi-edge cutting process that involves a large number of abrasive grains on the grinding wheel surface [7]. The grinding process is essentially a course in which a large number of discrete abrasive grains distributed on the surface of the grinding wheel interact with the processed component to achieve material removal, each abrasive grain on the surface of the grinding wheel makes a microscopic cutting into the worked material. Due to the characteristics of the grinding wheel manufacturing process, abrasive grains are arranged randomly on the circumference surface of the grinding wheel. The position and angle (the normal direction which is relative to the circumference surface of the grinding wheel in contact with the abrasive grain) of the abrasive grains are irregular and varied. In

addition, abrasive grains are consolidated on the grinding wheel, the spatial attitude of abrasive grains is also random. The random characteristics of abrasive grains are one of the reasons for the complexity of the grinding process [1]. Therefore, it is difficult to study the grinding mechanism through the complete grinding wheel, which is very unfavorable to the research promotion of the grinding process. The microscopic cutting of a single abrasive grain is a fundamental part of the grinding process, an effective means to understand the complex grinding processing mechanism, and its cutting action is the basis for material removal, thus researchers often choose the cutting process of a single abrasive grain for analysis in order to achieve the research of grinding wheel grinding mechanism [8].

Anderson et al. [9] compared the cutting action of two different single abrasive grain geometries by using experimental observations and a validated finite element model, and found that both tools required approximately the same energy to shear a chip from a workpiece when friction was subtracted from the specific energy for material removal. Gu et al. [10] were conducted single-abrasive-grain grinding experiments on SiCp/Al composites to determine the grinding forces at different grinding process parameters, established a prediction model for the single-abrasive-grain grinding force to study the influence of the grinding process parameters and grinding grain angle on the grinding force of SiCp/Al composite, and the PSO-SVM algorithm-based grinding force prediction model can accurately predict the grinding force of SiCp/Al composite and provides theoretical support for improved surface quality. Yin et al. [11] studied the effects of grinding speed on the

material removal mechanism of SiCf/SiC by single grain grinding, results indicate that increasing speed grinding could embrittle the material and enhance the breakage of fibers, both the groove surface quality and machining efficiency are improved by increasing speed grinding.

Grinding is a traditional precision machining method, which is carried out after the rough machining and makes the workpiece meet the requirements of high surface quality [12]. Grinding is a kind of abrasive processing technology, which means that abrasive play an important role in grinding. There are thousands of abrasive grains on the grinding wheel surface, which makes the grinding mechanism complicated [13]. Abrasive grains on the grinding wheel are the main part involved in material removal. As abrasive grains directly participate in the material removal process, their location and angle are considered to be important factors affecting the grinding surface quality, as well as the sharpness and wear resistance of abrasive grains themselves [14-15].In grinding, abrasive grains with rough and hard surfaces slide on the workpiece surface, make the surface material of the workpiece plastic deformation or fracture failure, and finally form the ground surface [16]. Accordingly, modeling and analyzing the abrasive model is conducive to grinding mechanism study and grinding quality prediction. In the previous grinding research, abrasive grains are usually considered as simple geometry to simplify the model. The spherical shape is the most widely used as an abrasive grain model [17-20]. Other simple geometries such as hexahedron and octahedron are often used as simplified models of abrasive grain [21-23]. However, there are little analyses in the relevant literature on the simplified model modeling

method and their cutting mechanism for truncated cone shape abrasive grain. Because the simple single abrasive grain model lacks the random characteristics of abrasive grain, so, the random angle of the single abrasive grain model has obvious advantages in grinding research. In the field of grinding, due to the complexity of the model, few studies are using random angles in a single abrasive grain model.

At present, the methods for single abrasive grain cutting mechanism study are mainly focused on experimental research or finite element software simulation research, and the theoretical research on single abrasive grain cutting mechanism is relatively less. Based on the above, a theoretical model of cutting mechanism based on randomly deflected truncated cone shape single abrasive grain was established considering the grinding parameters and deflection parameters comprehensively. The fundamental theory research on the cutting behavior of a single abrasive grain was carried out, and further lay a foundation for exploring the grinding mechanism of the grinding wheel.

2 Random deflection truncated cone shape single abrasive grain cutting model

2.1 Establish workpiece coordinate system

In order to describe the cutting process of the single abrasive grain with a randomly deflected angle. A coordinate system was established on the surface of the workpiece in first, with the length of the workpiece as l_w, the width as b_w, and the height as z_w, the subscript "w" represents the workpiece. The x-axis direction is the length direction of the workpiece, the y-axis direction is the width direction of the workpiece, and the z-axis direction is the height direction of the workpiece, the origin

of the coordinate system O_w is located at the center of the upper surface of the workpiece. Δwx denotes the discrete step size for discretization in the length direction of the workpiece, Δwy denotes the discrete step size for discretization in the width direction of the workpiece. $x_w(i)$ denotes the x-coordinate of the location for the i-th discrete point in the length direction of the workpiece, and $y_w(j)$ denotes the y-coordinate of the location for the j-th discrete point in the width direction of the workpiece.

The discretization process of $x_w(i)$ is expressed by the formula below:

$$x_w(i) = -\frac{l_w}{2} : \Delta wx : \frac{l_w}{2} \tag{1}$$

The discretization process of $y_w(j)$ is expressed by the formula below:

$$y_w(j) = -\frac{b_w}{2} : \Delta wy : \frac{b_w}{2} \tag{2}$$

$X_w(i, j)$ was denoted to express the x-coordinate of all discrete points on the upper surface of the workpiece, $y_w(i, j)$ was denoted to express the y-coordinates of all discrete points on the upper surface of the workpiece, and $z_w(i, j)$ was denoted to express the z-coordinates of all discrete points on the upper surface of the workpiece, and:

$$\begin{cases} x_w(i,j) = x_w(i) \\ y_w(i,j) = y_w(j) \\ z_w(i,j) = 0 \end{cases} \tag{3}$$

Up to now, the workpiece coordinate system constructed completely, as shown in Fig.1.

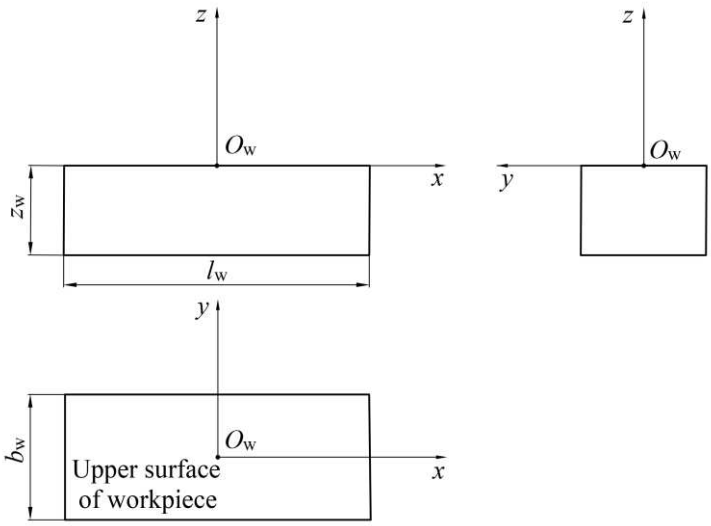

Fig.1. The three views of the workpiece coordinate system.

2.2 Cutting process modeling

The diameter of the grinding wheel is d_s, the radius is r_s, the circumferential linear velocity of the grinding wheel is v_s, the circumferential angular velocity of the grinding wheel is ω_s, the center of the grinding wheel is O_s, the grinding depth of the grinding wheel is a_e, and the subscript "s" represents the grinding wheel, x_{so}, y_{so}, and z_{so} denote the coordinates of the center of the grinding wheel circle on the x-axis, y-axis, and z-axis, respectively. After establishing the workpiece coordinate system, the relative motion of the abrasive grain and the workpiece was transformed into the workpiece did not move, and the grinding wheel moved, at this time, the feed motion of the workpiece was transformed into the workpiece did not move and the grinding wheel axis moved along the x-axis direction. The feed speed of the grinding wheel is v_f, and $v_w=-v_f$. Consequently, the abrasive grain moving trajectory was a combination in the rotational motion of the grinding wheel and the feed motion of the workpiece. The grinding wheel grinds the workpiece as shown in Fig.2.

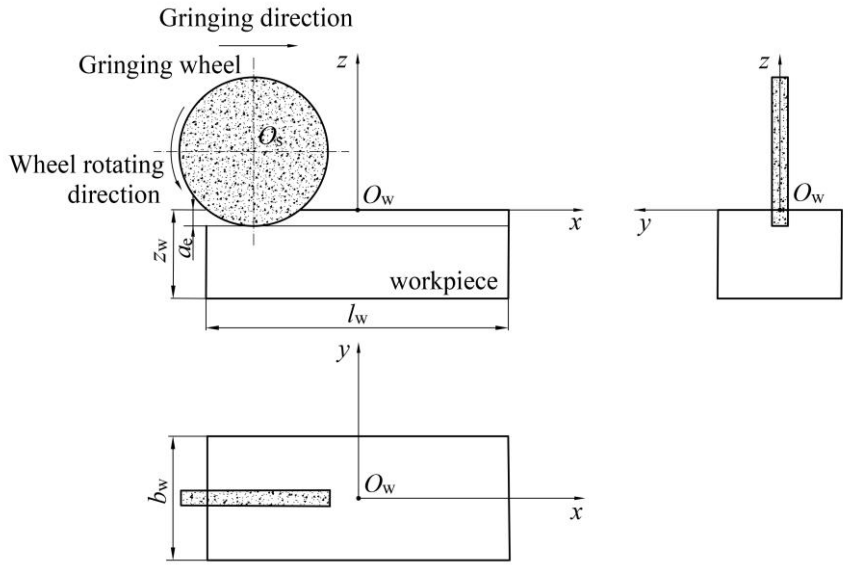

Fig.2. The three views of grinding wheel working conditions.

The abrasive grain was defined as a truncated cone shape, h was represented to the cutting depth of the abrasive grain, h_{max} was represented to the maximum cutting depth of the abrasive grain, h_g was represented to the height of the abrasive grain, and h_{gz} was represented to the height of the conical geometry (hereinafter called cone) formed by the truncated cone abrasive grain as a reference, the subscript “g” indicates the abrasive grain, and the subscript “z” indicates the cone, d_{gm} was represented to the diameter of the abrasive grain's large circle, d_{gn} was represented to the diameter of the abrasive grain's small circle, the subscript “m” indicates the large circular surface of the abrasive grain, and the subscript “n” indicates the small circular surface of the abrasive grain. According to the geometric relationship of the truncated cone shape abrasive grain, h_{gz} could be expressed by h_g, d_{gm}, and d_{gn}, which were expressed by Eq.(4):

$$h_{gz} = \frac{d_{gm} h_g}{d_{gm} - d_{gn}} \tag{4}$$

The parameter β was denoted to express the half-top angle of the cone (in radians)

and was expressed by the formula:

$$\beta = \arctan\left(\frac{d_{\mathrm{gm}}}{2h_{\mathrm{gz}}}\right) \tag{5}$$

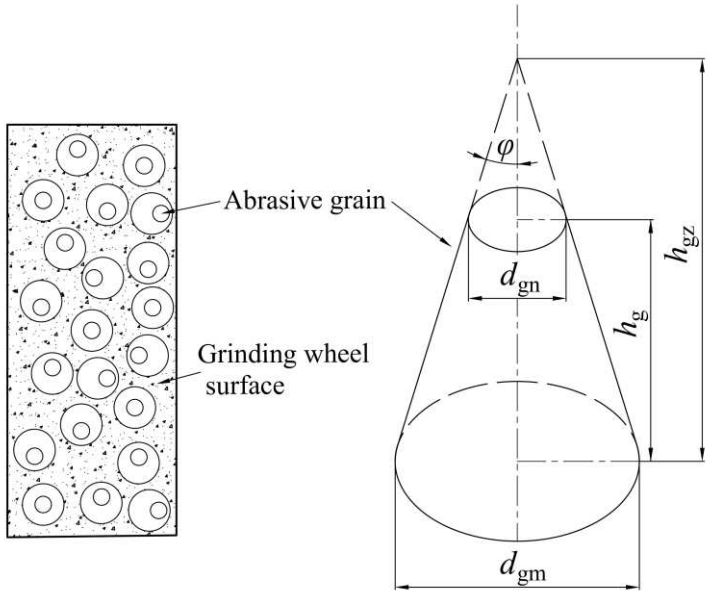

Fig.3. The position and parameters of abrasive grain.

The parameter φ was indicated to express the cut-in angle or cut-out angle of the grinding wheel cutting workpiece process, φ could be expressed in Eq.(6), and shown in Fig.4.

$$\varphi = \arccos\left(\frac{z_{\mathrm{so}}}{r_{\mathrm{s}} + h_{\mathrm{gz}}}\right) \tag{6}$$

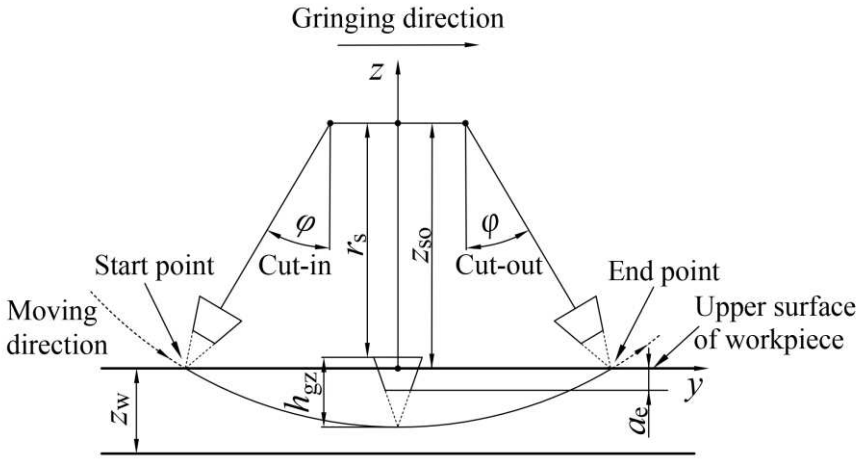

Fig.4. Abrasive grain cut-in and cut-out position.

The parameter t was indicated to express the cutting time used by the abrasive grain from cut-in to cut-out of the workpiece, $t_{\min}$ is the time when the abrasive grain starts cutting, $t_{\max}$ is the time when the abrasive grain ends cutting, n_{t} denotes the number of discrete steps in cutting time, Δt denotes the discrete step size for discrete processing of the cutting time, t_{i} denotes the time corresponding to the i-th discrete point in the cutting time of the abrasive grain, according to the cutting process of a single abrasive grain:

$$\begin{cases} t_{\min} = 0 \\ t_{\max} = \dfrac{2\varphi}{\omega_{\mathrm{s}}} \\ \Delta t = \dfrac{t_{\max}}{n_{\mathrm{t}}} \\ t_{\mathrm{i}} = t_{\min} : \Delta t : t_{\max} \end{cases} \tag{7}$$

The v_{f} is positive when it coincides with the positive direction of the x-axis, the length traveled by the center of the wheel in the x-axis direction at the ends cutting time was expressed by l_{sox}, the formula was below:

$$l_{\mathrm{sox}} = v_{\mathrm{f}} t_{\max} \tag{8}$$

At the time of t_{i}, the coordinates of the center of the grinding wheel circle on the x-axis, y-axis, and z-axis were:

$$\begin{cases} x_{\mathrm{so}} = -\dfrac{l_{\mathrm{sox}}}{2} + v_{\mathrm{f}} t_{\mathrm{i}} \\ y_{\mathrm{so}} = 0 \\ z_{\mathrm{so}} = r_{\mathrm{s}} + h_{\mathrm{g}} - a_{\mathrm{e}} \end{cases} \tag{9}$$

The trajectory of the cutting motion of the abrasive grain was shown in Fig.5.

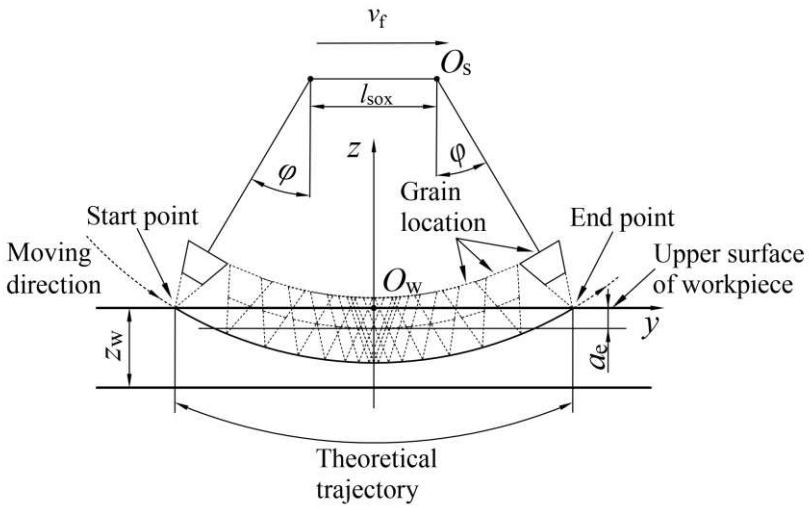

Fig.5. The grain moving trajectory.

The position of the abrasive grain was changed by the rotation of the grinding wheel, the center of the large circle of the grinding grain is O_{gm}, and the top point of the cone is A_{gz}, x_{gm}, y_{gm}, and z_{gm} denoted the x, y, and z coordinates of O_{gm}, respectively, and x_{gza}, y_{gza}, and z_{gza} denoted the x, y, and z coordinates of A_{gz}, respectively. Then, at the time of t_i, the coordinates of O_{gm} and A_{gz} were:

$$\begin{cases} x_{gm} = x_{so} \pm r_s \sin(\varphi - \omega_s t_i) \\ y_{gm} = y_{so} \\ z_{gm} = z_{so} - r_s \cos(\varphi - \omega_s t_i) \end{cases} \tag{10}$$

$$\begin{cases} x_{gza} = x_{so} \pm (r_s + h_{gz}) \sin(\varphi - \omega_s t_i) \\ y_{gza} = y_{so} \\ z_{gza} = z_{so} - (r_s + h_{gz}) \cos(\varphi - \omega_s t_i) \end{cases} \tag{11}$$

where "+" represents down-grinding, and "–" represents up-grinding.

The geometric relationship of the above formulas was as shown in Fig.6, Fig.6(a) shows up-grinding, and Fig.6(b) shows down-grinding.

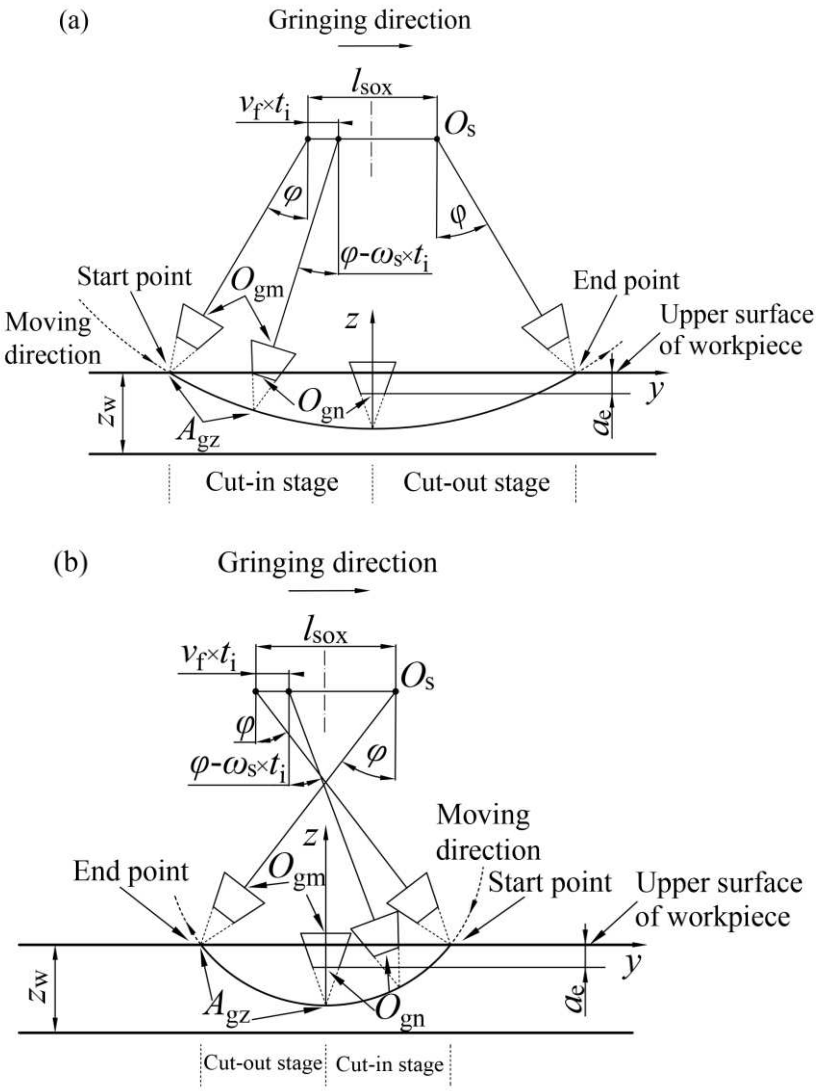

Fig.6. Single abrasive grain cutting process and geometric relationship between wheel and workpiece. (a) up-grinding, (b) down-grinding.

The position of the abrasive grain would change under the deflection of its axis around O_{gm}, and the abrasive grain was coaxial with the cone, δ_1 was defined to express the deflection angle of the central axis for the cone in the plane perpendicular to the plane xOz and passing through the line O_s-O_{gm}, the subscript "1" indicates the plane that perpendicular to the plane xOz and passing through the line O_s-O_{gm}, the angle value was positive when the δ_1 deflection direction is the same as the positive direction of the y-axis, and the range of the angle is in $[-\pi/2, \pi/2]$, after deflection, the

projection line of the axis in the xOz plane was co-linear with the line O_s-O_{gm}, as shown in Fig.7.

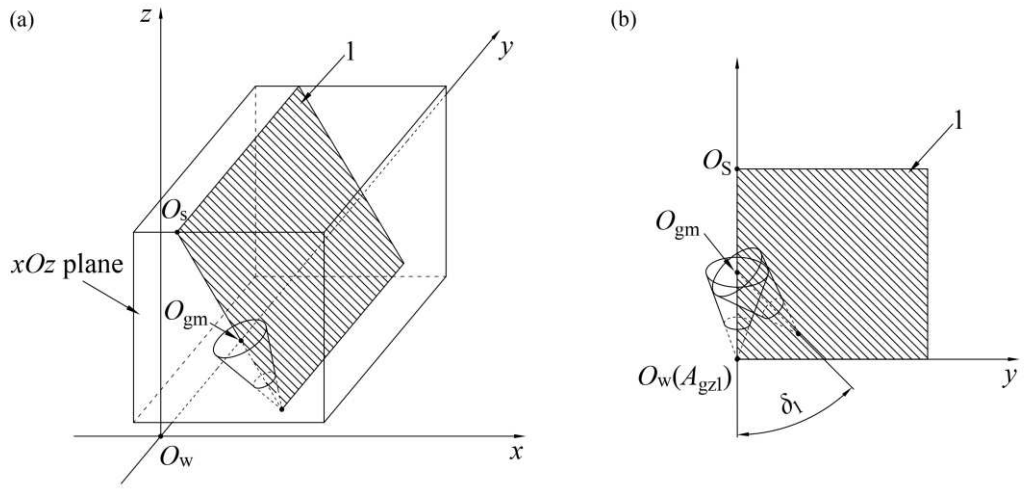

Fig.7. Schematic diagram of the grinding grain deflection angle δ_1. (a) plane 1 axonometric view, (b) plane 1 front view .

After deflecting angle δ_1, δ_2 was defined to express the deflection angle by the rotation of the abrasive grain axis projected straight line in the xOz plane around the y-axis, the subscript 2 indicates the plane of rotation parallel to the xOz plane, the angle value was positive when the δ_2 deflection direction is the same as the positive direction of the x-axis, and the range of the angle is in $[-\pi/2, \pi/2]$, as shown in Fig.8.

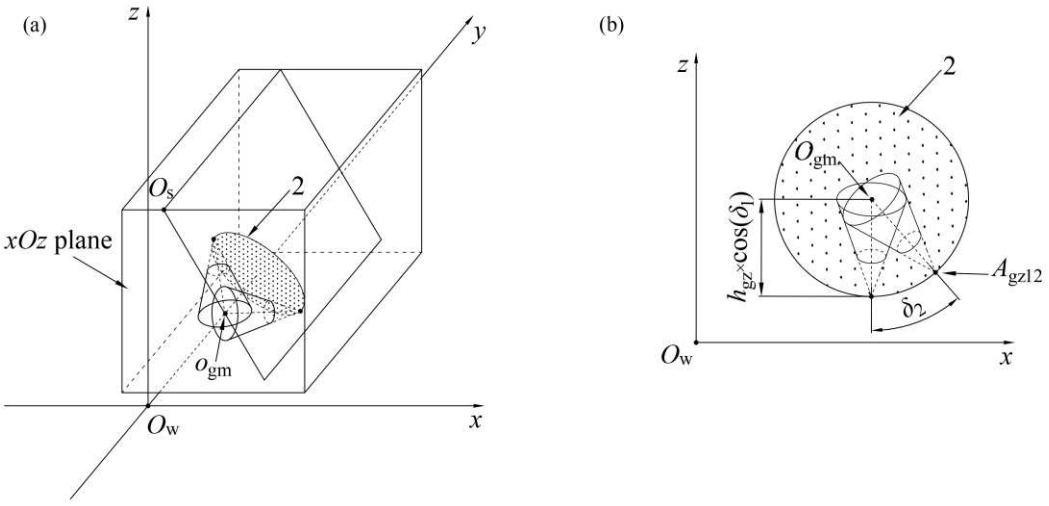

Fig.8. Schematic diagram of the grinding grain deflection angle δ_2. (a) plane 1 axonometric view,

(b) plane 1 front view .

The position of A_{gz} was transformed to A_{gz1} when the deflected angle was δ_1, x_{gza1}, y_{gza1}, and z_{gza1} denoted the x, y, and z coordinates of A_{gz1}, respectively. So, at the moment t_i, the coordinates of A_{gz1} were:

$$\begin{cases} x_{gza1} = x_{so} \pm (r_s + h_{gz}\cos\delta_1)\sin(\varphi - \omega_s t_i) \\ y_{gza1} = y_{so} + h_{gz}\sin\delta_1 \\ z_{gza1} = z_{so} - (r_s + h_{gz}\cos\delta_1)\cos(\varphi - \omega_s t_i) \end{cases} \tag{12}$$

where "+" represents down-grinding, and "–" represents up-grinding.

On the basis of a deflected angle δ_1, the position of A_{gz1} was transformed to A_{gz12}, when the deflected angle was δ_2, x_{gza12}, y_{gza12}, and z_{gza12} denoted the x, y, and z coordinates of A_{gz12}, respectively. So, at the moment t_i, the coordinates of A_{gz12} were:

$$\begin{cases} x_{gza12} = x_{gm} \pm h_{gz}\cos\delta_1\sin(\varphi - \omega_s t_i \pm \delta_2) \\ y_{gza12} = y_{gza1} \\ z_{gza12} = z_{gm} - h_{gz}\cos\delta_1\cos(\varphi - \omega_s t_i \pm \delta_2) \end{cases} \tag{13}$$

where "+" represents down-grinding, and "–" represents up-grinding.

The workpiece topography could be represented by a matrix of points with different heights [24]. The number of discrete points in the length and width directions of the workpiece were denoted by n_l and n_b, respectively. The height of each point was stored in a two dimensional matrix $Z[n_l,n_b]$. Before grinding, the height of all the points was zero, i.e., all discrete points were on the surface of the workpiece. The distance between two adjacent points was 1/100 of the d_{gm}:

$$\begin{cases} \Delta wx = \dfrac{1}{100} d_{gm} \\ \Delta wy = \dfrac{1}{100} d_{gm} \end{cases} \tag{14}$$

The point numbers were:

$$\begin{cases} n_{\mathrm{l}} = \left[\dfrac{l_{\mathrm{w}}}{\Delta wx} \right] \\ n_{\mathrm{b}} = \left[\dfrac{b_{\mathrm{w}}}{\Delta wy} \right] \end{cases} \tag{15}$$

The square brackets indicate rounding.

O_{gm} was selected as the reference point in the cutting process., at ti, the coordinates of O_{gm} could be expressed by ($x_{\mathrm{gm,i}}$, $y_{\mathrm{gm,i}}$, $z_{\mathrm{gm,i}}$). According to the abrasive grain position, the limit value $X_{\min}$, $X_{\max}$, $Y_{\min}$, $Y_{\max}$ of the coordinates on the workpiece surface points, for heights that might be affected by the abrasive grain, could be found in the matrix Z, and could be easily determined by:

$$\begin{cases} X_{\min} = [x_{\mathrm{gm,i}} - h_{\mathrm{gz}}] \\ X_{\max} = [x_{\mathrm{gm,i}} + h_{\mathrm{gz}}] \\ Y_{\min} = [y_{\mathrm{gm,i}} - h_{\mathrm{gz}}] \\ Y_{\max} = [y_{\mathrm{gm,i}} + h_{\mathrm{gz}}] \end{cases} \tag{16}$$

The square brackets indicate rounding.

The region of [$X_{\min}$, $X_{\max}$]×[$Y_{\min}$, $Y_{\max}$] was scanned in the program point-by-point to calculate.

2.3 Cutting process calculation

In the cutting process of the abrasive grain, the workpiece was defined as an ideal body (without considering the effect of deformation, residual stress, etc.). And the cutting was simply regarded as the relative motion of the abrasive grain and the workpiece, i.e., the type of contacting abrasive grain in the grinding arc was only cutting abrasive grain, and the interference part between the abrasive grain and the workpiece in the process of movement was all regarded as the removal of material. After being cut by the abrasive grain, the z-coordinate of the cut point on the

workpiece surface would change, while x-coordinate and y-coordinate stay the same, x_w, y_w and z_w denote the x, y and z coordinates of discrete points on the workpiece surface. According to the analysis above, it can solve the new z-axis coordinates of the cut point on the workpiece surface after abrasive grain cutting, and use z_{wn} to represent. The position of discrete points on the workpiece surface after cutting were in two cases, the first situation was located on the truncated conical surface of the abrasive grain, and the second situation was located on the small circular surface of the abrasive grain.

In the first case, the axis of the cone after deflection δ_1 and δ_2, denoted by r_1, and could be expressed as:

$$r_1 = [x_{gza12} - x_{gm}, y_{gza12} - y_{gm}, z_{gza12} - z_{gm}] \tag{17}$$

The new position and its coordinates of the cut point were expressed in terms of $C_{gz}(x_w, y_w, z_1)$, the straight line C_{gz}-A_{gz12} denoted by r_2, and could be expressed as:

$$r_2 = [x_{gza12} - x_w, y_{gza12} - y_w, z_{gza12} - z_1] \tag{18}$$

The angle between the r_1 and r_2 was equal to the half-top angle of the cone, could be expressed as:

$$\arccos \frac{r_1 \cdot r_2}{|r_1|\,|r_2|} = \beta \tag{19}$$

Organized Eq. (19), and obtained:

$$\cos^2 \beta = \frac{(r_1 \cdot r_2)^2}{|r_1|^2 |r_2|^2} \tag{20}$$

Since the only unknown variable in Eq. (20) was z_1, thus, the constant part in Eq. (20) could define by other characters:

$$\begin{cases} E_1 = \cos^2\beta |r_1|^2 \\ E_2 = (x_{\mathrm{gza}12} - x_{\mathrm{gm}})(x_{\mathrm{gza}12} - x_{\mathrm{w}}) + (y_{\mathrm{gza}12} - y_{\mathrm{gm}})(y_{\mathrm{gza}12} - y_{\mathrm{w}}) \\ E_3 = (z_{\mathrm{gza}12} - z_{\mathrm{gm}}) z_{gza12} \\ E_4 = z_{\mathrm{gza}12} - z_{\mathrm{gm}} \\ E_5 = (x_{\mathrm{gza}12} - x_{\mathrm{w}})^2 + (y_{\mathrm{gza}12} - y_{\mathrm{w}})^2 + z_{\mathrm{gza}12}^2 \\ E_6 = E_4^2 - E_1 \\ E_7 = 2E_1 z_{\mathrm{gza}12} - 2(E_2 + E_3)E_4 \\ E_8 = (E_2 + E_3)^2 - E_1 E_5 \end{cases} \tag{21}$$

The formula could be transformed as:

$$E_6 z_1^2 + E_7 z_1 + E_8 = 0 \tag{22}$$

The new z-axis coordinate values would be obtained after computing Eq. (22), which were named z_{11} and z_{12}, due to the $\cos^2\beta$ have the following characteristics in Eq. (20), as shown in Fig.9.

$$\cos^2\beta = (-\cos(\pi - \beta))^2 = \cos^2(\pi - \beta) \tag{23}$$

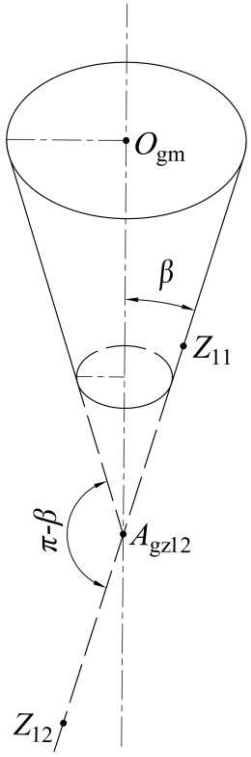

Fig.9. The location of z_{11} and z_{12} on the conic surface .

From Eq. (23) and Fig.9, the angle between r_1 and r_2 was either β or $(\pi-\beta)$,

corresponding to the two solutions z_{11} and z_{12}. Because the new position makes the angle β between r_1 and r_2, thus, as the unqualified solution z_{12} should be discarded.

In the second case, as known from the previous that r_1 was the normal vector of the large and small circular surfaces of the abrasive grain. $C_{\mathrm{gm}}(x, y, z)$ were expressed at any point and its coordinates on the large circular surface of the abrasive grain. $L(x, y, z)$ was the plane formula of the large circular surface. From the formula of the plane equation:

$$\begin{aligned} L(x,y,z):&(x_{\mathrm{gm}}-x_{\mathrm{gza}})\,(x-x_{\mathrm{gm}})+(y_{\mathrm{gm}}-y_{\mathrm{gza12}})\,(y-y_{\mathrm{gm}}) \\ &+(z_{\mathrm{gm}}-z_{\mathrm{gza12}})\,(z-z_{\mathrm{gm}})=0 \end{aligned} \tag{24}$$

Organized Eq. (24), and obtained:

$$\begin{aligned} L(x,y,z):&(x_{\mathrm{gm}}-x_{\mathrm{gza12}})x+(y_{\mathrm{gm}}-y_{\mathrm{gza12}})y+(z_{\mathrm{gm}}-z_{\mathrm{gza12}})z \\ -&((x_{\mathrm{gm}}-x_{\mathrm{gza12}})x_{\mathrm{gm}}+(y_{\mathrm{gm}}-y_{\mathrm{gza12}})y_{\mathrm{gm}}+(z_{\mathrm{gm}}-z_{\mathrm{gza12}})z_{\mathrm{gm}})=0 \end{aligned} \tag{25}$$

The new position and its coordinates of the cut point were expressed in terms of $C_{\mathrm{gn}}(x_{\mathrm{w}}, y_{\mathrm{w}}, z_2)$. The distance from the point C_{gn} to the large circular surface of the abrasive grain was equal to h_{g}. So:

$$h_{\mathrm{g}}=\frac{|L(x_{\mathrm{w}},y_{\mathrm{w}},z_2)|}{\sqrt{(x_{\mathrm{gm}}-x_{\mathrm{gza12}})^{2}+(y_{\mathrm{gm}}-y_{\mathrm{gza12}})^{2}+(z_{\mathrm{gm}}-z_{\mathrm{gza12}})^{2}}} \tag{26}$$

In the Eq. (25):

$$\begin{aligned} L(x_{\mathrm{w}},y_{\mathrm{w}},z_2):&(x_{\mathrm{gm}}-x_{\mathrm{gza12}})x_{\mathrm{w}}+(y_{\mathrm{gm}}-y_{\mathrm{gza12}})y_{\mathrm{w}}+(z_{\mathrm{gm}}-z_{\mathrm{gza12}})z_2 \\ -&((x_{\mathrm{gm}}-x_{\mathrm{gza12}})x_{\mathrm{gm}}+(y_{\mathrm{gm}}-y_{\mathrm{gza12}})y_{\mathrm{gm}}+(z_{\mathrm{gm}}-z_{\mathrm{gza12}})z_{\mathrm{gm}}) \end{aligned} \tag{27}$$

Since the only unknown variable in Eq. (26) was z_2, thus, the constant part in Eq. (26) could define by other characters:

$$\begin{cases} F_1 = (x_{\mathrm{gm}} - x_{\mathrm{gza12}})x_{\mathrm{w}} + (y_{\mathrm{gm}} - y_{\mathrm{gza12}})y_{\mathrm{w}} \\ F_2 = (x_{\mathrm{gm}} - x_{\mathrm{gza12}})x_{\mathrm{gm}} + (y_{\mathrm{gm}} - y_{\mathrm{gza12}})y_{\mathrm{gm}} + (z_{\mathrm{gm}} - z_{\mathrm{gza12}})z_{\mathrm{gm}} \\ F_3 = z_{\mathrm{gm}} - z_{\mathrm{gza12}} \\ F_4 = \sqrt{(x_{\mathrm{gm}} - x_{\mathrm{gza12}})^2 + (y_{\mathrm{gm}} - y_{\mathrm{gza12}})^2 + (z_{\mathrm{gm}} - z_{\mathrm{gza12}})^2} \\ F_5 = 2(F_1 - F_2)F_3 \\ F_6 = (F_1 - F_2)^2 - F_4^2 h_{\mathrm{g}}^2 \end{cases} \tag{28}$$

The formula could be transformed as:

$$F_3^2 z_2^2 + F_5 z_2 + F_6 = 0 \tag{29}$$

The new z-axis coordinate values would be obtained after computing Eq. (29), which were named z_{21} and z_{22}, as shown in Fig.10.

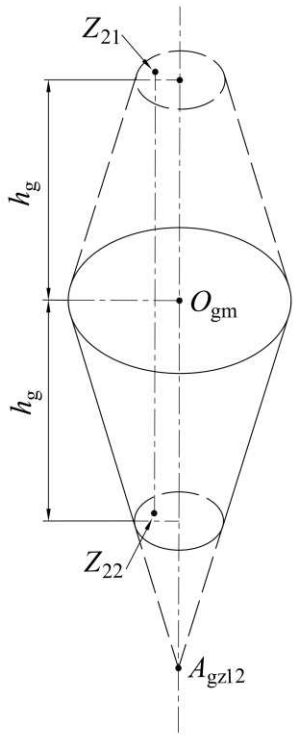

Fig.10. The location of z_{21} and z_{22} on the small circular surface .

From Fig.10, the plane with distance h_{g} to the large circular surface of the abrasive grain were the small circular surface plane and its symmetrical mirror plane about the large circular surface. The solution in the mirror plane was z_{21} and the solution in the small circular plane was z_{22}. Because the new location was on the small

circular surface of abrasive grain, thus, as the unqualified solution z_{21} should be discarded.

Based on the above, the geometric relationship between $z_{11}$and z_{22} was as shown in Fig.11.

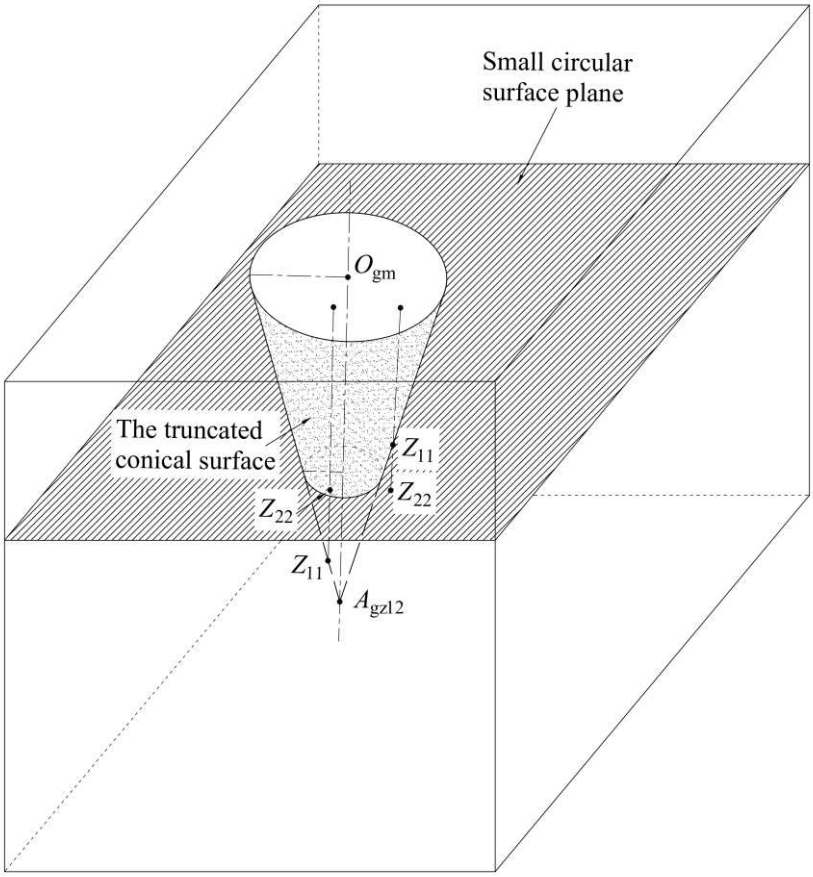

Fig.11. The geometric relationship between solutions.

According to the geometric relationship represented in Fig.11, it was clear that:

$$z_{wn} = \max(z_{11}, z_{22}) \tag{30}$$

The discrete points on the workpiece surface can be divided into the cut and uncut points. After the abrasive grain cutting, the z-coordinate of the cut point on the workpiece surface was become z_{wn}, while the uncut point remain the same.

2.4 Case model calculation and study

According to Eqs. (7)-(13), the time interval [t_{min},t_{max}] had been discretized, a series of discrete points on the abrasive grain cutting trajectory could be obtained. The adjacent time points could be expressed by t_i and t_{i+1}, t_{i+1}=t_i+Δt. The coordinates of the corresponding A_{gz12} positions were $A_{gz12,i}(x_{gza12,i},y_{gza12,i},z_{gza12,i})$ and $A_{gz12,i+1}(x_{gza12,i+1},y_{gza12,i+1},z_{gza12,i+1})$, then the distance between the two positions was, used Δl_i to express:

$$\Delta l_i = \overline{A_{gz12,i}A_{gz12,i+1}} = \sqrt{(x_{gza12,i+1}-x_{gza12,i})^2+(y_{gza12,i+1}-y_{gza12,i})^2+(z_{gza12,i+1}-z_{gza12,i})^2} \tag{31}$$

The length of the abrasive grain cutting trajectory was, used L_g to express:

$$L_g = \lim_{\Delta t \to 0} \sum_{t=0}^{t=max} \Delta l_i \tag{32}$$

The following were calculation examples and verification:

According to Eqs. (1)-(13), a calculation program was compiled and run with the parameters shown in Table 1. The calculation results are shown in Table 2. The calculation results in Table 2 represent verification of this work. The calculation results were compared with the theoretical model proposed by S.Malkin [12] for common plane surface grinding conditions. It should be noted that the grinding contact length obtained by Malkin's formula was for an abrasive grain moving from the lowest point to the endpoint of the cut-out stage, taking the up-grinding as an example. Therefore, the abrasive grain cutting trajectory length calculated in this work was twice that of Malkin's formula.

Malkin's formula:

$$L_{\mathrm{k}}=\left(1\pm\frac{v_{\mathrm{w}}}{v_{\mathrm{s}}}\right)\sqrt{a_{\mathrm{e}}d_{\mathrm{s}}} \tag{33}$$

where "+" represents down-grinding, and "–" represents up-grinding.

The grinding depth a_{e} in Eq.(13) needed to be replaced by the A_{gz12}'s cutting depth $a_{\mathrm{e}}+h_{\mathrm{gz}}-h_{\mathrm{g}}$, because the cutting depths were different for different A_{gz12}. Then Eq. (33) was become the following:

$$L_{\mathrm{k}}=\left(1\pm\frac{v_{\mathrm{w}}}{v_{\mathrm{s}}}\right)\sqrt{(a_{\mathrm{e}}+h_{\mathrm{gz}}-h_{\mathrm{g}})d_{\mathrm{s}}} \tag{34}$$

The calculation results were compared under the parameters of Group No.1 and Group No.2, as shown in Table 2.

Table 1. Typical grinding parameters and value ranges.

Group	Grinding parameters	Typical value	Value range
Group No.1	Wheel speed, v_{s}, (m/s)	20	10，15，20，25，30
Group No.2	Wheel diameter, d_{s}, (mm)	200	100，150，200，250，300
Group No.3	Workpiece feed speed, v_{ω}, (mm/s)	20	10，15，20，25，30
Group No.4	Grain's cutting depth, h, (μm)	50	30，40，50，60，70
Group No.5	Deflection angle, δ_1, (rad)	0	−0.2，−0.1，0，0.1，0.2
Group No.6	Deflection angle, δ_2, (rad)	0	−0.2，−0.1，0，0.1，0.2
Other parameters: l_{w}=10mm, b_{w}=0.3mm, d_{gm}=0.1mm, d_{gn}=0.03mm, h_{g}=0.1mm			

Table 2. Verification of the numerical method.

Group No.1	Grinding methods	Wheel speed, v_{s}(m/s)	L_{g}, mm	$2L_{\mathrm{k}}$, mm	Error, $(L_{\mathrm{g}}-2L_{\mathrm{k}})/(2L_{\mathrm{k}})$, %
d_{s}=200 mm v_{ω}=20 mm/s h=50 μm δ_1=0 rad δ_2=0 rad	Down-grinding	10	8.6085	8.6017	0.079485
		15	8.6143	8.6074	0.079369
		20	8.6171	8.6103	0.079311
		25	8.6188	8.6120	0.079276
		30	8.6200	8.6132	0.079253
	Up-grinding	10	8.6430	8.6362	0.078791
		15	8.6372	8.6304	0.078906
		20	8.6343	8.6275	0.078964
		25	8.6326	8.6258	0.078998
		30	8.6315	8.6247	0.079021
Group No.2	Grinding	Wheel diameter,	L_{g}, mm	$2L_{\mathrm{k}}$, mm	Error,

	methods	d_s(mm)			$(L_g-2L_k)/(2L_k)$, %
v_s=20 m/s v_ω=20 mm/s h=50 μm δ_1=0 rad δ_2=0 rad	Down-grinding	100	6.0981	6.0884	0.158560
		150	7.4646	7.4567	0.105730
		200	8.6171	8.6103	0.079311
		250	9.6327	9.6266	0.063454
		300	10.5510	10.5454	0.052881
	Up-grinding	100	6.1102	6.1006	0.157870
		150	7.4795	7.4717	0.105270
		200	8.6343	8.6275	0.078964
		250	9.6520	9.6459	0.063176
		300	10.5721	10.5665	0.052649

As shown in Table 2, the comparison errors were very small (<0.16%). Thus, the proposed numerical method was verified.

According to the above analysis, after all of the points in the region were processed, the ground surface topography could be obtained. When each parameter was the same as Table 1 and the grinding method was up grinding, Fig.12 and Fig.13 show the calculation results.

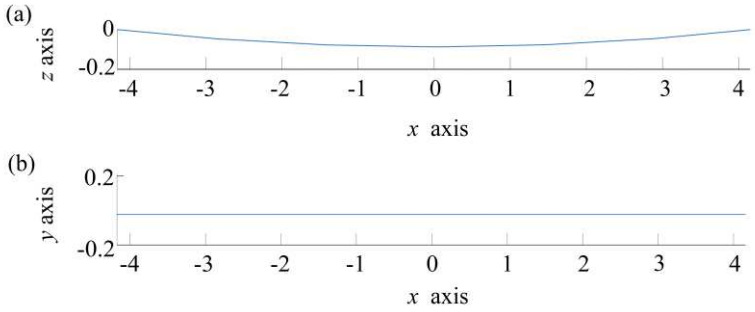

Fig.12. Grain moving trajectory calculation results. (a) front view, (b) top view.

Fig.12(a) and (b) show the front and top views of the A_{gz} moving trajectory.

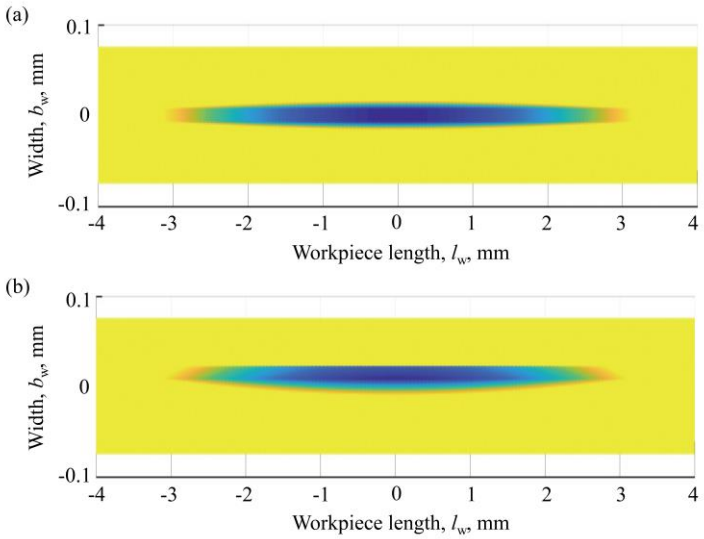

Fig.13. Top view of workpiece surface topography calculation results. (a) δ_1=0 rad, (b) δ_1=0.1 rad.

Fig.13(a) and (b) show the top views of the simulated 3D ground surface, (a) δ_1=0 rad (b) δ_1=0.1 rad. The deeper the color is, the greater the cut depth was.

The area of the workpiece's upper surface was denoted by p_w, n_w denoted the number of all discrete points on the upper surface of the workpiece, p_{we} denoted the number of all discrete points on the upper surface of the workpiece. Based on the cutting process model, the formulas were below:

$$\begin{cases} p_w = l_w b_w \\ n_w = n_l n_b \\ p_{we} = \dfrac{p_w}{n_w} \end{cases} \tag{35}$$

Material removal volume was denoted by *MRV*, represented the sum of the cutting volume of all discrete points on the workpiece. Before grinding, the initial height value of all the points was zero, after grinding, the *z*-coordinate of the cut point on the workpiece surface was become z_{wn}, while the uncut point remain the same. Therefore, the *MRV* of the single abrasive grain cutting could be expressed as follows:

$$MRV = \lim_{\substack{\Delta wx \to 0 \\ \Delta wy \to 0}} \sum_{i=-\frac{l_w}{2}}^{i=\frac{l_w}{2}} \sum_{j=-\frac{b_w}{2}}^{j=\frac{b_w}{2}} p_{we} |z_w(i,j) - 0| \tag{36}$$

The material removal rate was denoted by *MRR*, represented the cutting volume of material removal per unit time. The *MRR* of the single abrasive grain cutting can be expressed as follows:

$$MRR = \frac{MRV}{t_{max} - t_{min}} \tag{37}$$

When each parameter was the same as Table 1 (without value range) and the grinding method was up grinding, The *MRV* was 9.0023×10^{-3} mm^3 and the *MRR* was 20.9028 mm^3/s by calculation.

In previous related studies, the cutting depth of the abrasive grain *h*, also known as the undeformed chip thickness, is a very important Parameter in the modeling of grinding processes. Many researchers have used *h* to study grinding quality, removal and chip formation mechanisms, etc. For the single abrasive grain cutting studied in this paper, h_{max}, i.e., the maximum unshaped chip thickness, is equal to a_e, and in the process of abrasive grain cutting, the undeformed chip thickness had a large relationship with the grinding method, *MRV*, and *MRR*. Therefore, in order to investigate the cutting mechanism of single abrasive grain in depth, improve the surface quality of workpiece, it is necessary to calculate the undeformed chip thickness and shape of the single abrasive grain cutting model.

The workpiece was partitioned by a series of planes perpendicular to the *x*-axis, the distance between adjacent planes was equal to *Δwx*, the resulting cross-sections were the undeformed chip section shape and in which the thickness of the undeformed

chip can be displayed. A Matlab calculation program was prepared, each parameter was the same as Table 1 and the grinding method was up grinding, then, the undeformed chip section shape could be obtained, as shown in Fig.14.

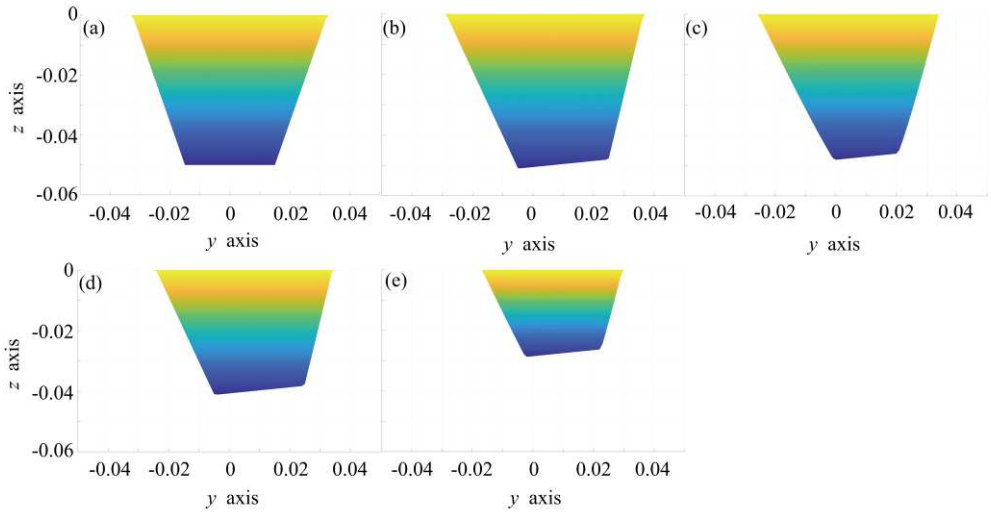

Fig.14. The undeformed chip section shapes. (a) x=0 mm section, δ_1=0 rad, (b) x=0 mm section, δ_1=0.1 rad, (c) x=0.701 mm section, δ_1=0.1 rad, (d) x=1.401 mm section, δ_1=0.1 rad, (e) x=2.101 mm section, δ_1=0.1 rad.

The undeformed chip shape was obtained by placing all the cross-sections of the workpiece in one diagram, as shown in Fig.15.

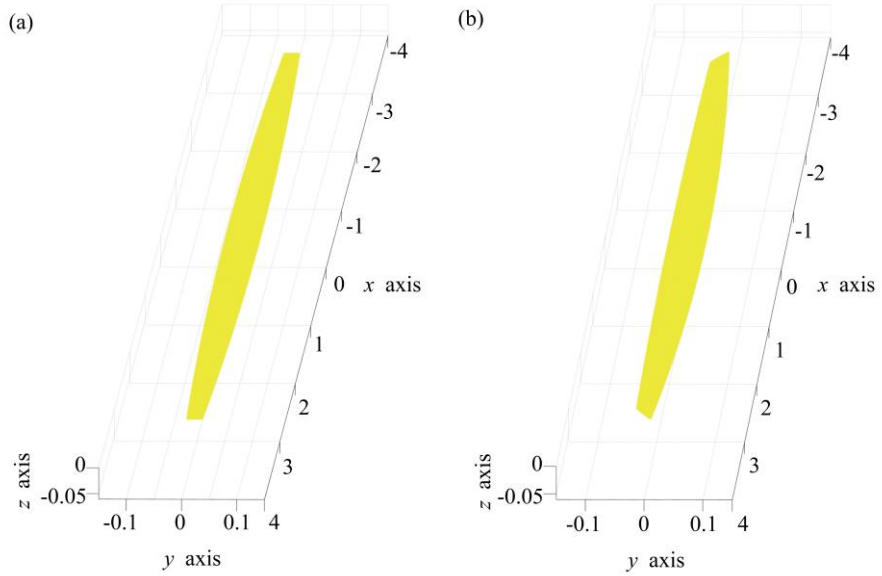

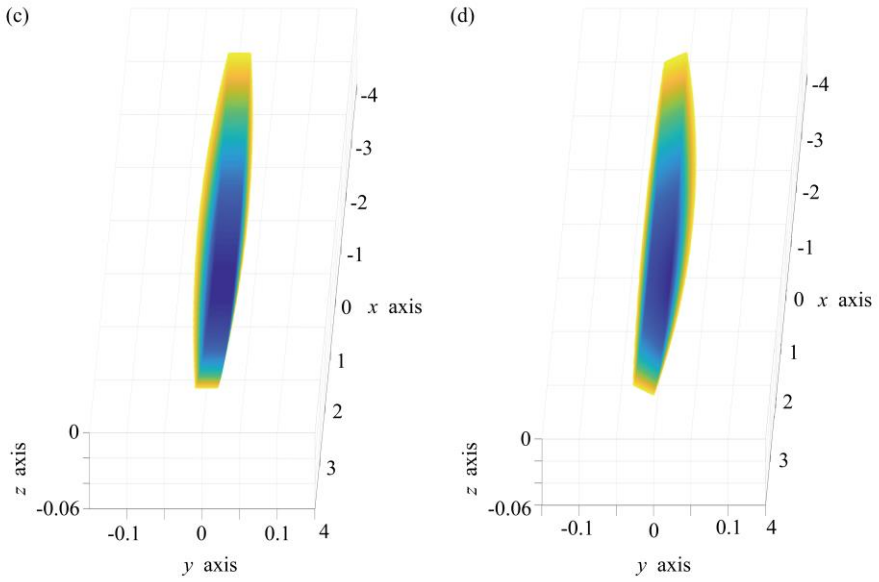

Fig.15. The undeformed chip shapes. (a) (c) δ_1=0 rad, (b) (d) δ_1=0.1 rad.

Fig.15(a) and (b) show the *z*-axis positive direction views of the undeformed chip shapes, (c) and (d) show the *z*-axis negative direction views of the undeformed chip shapes.

As can be seen from Fig.13 and Fig.15, for the single abrasive grain cutting, the undeformed chip shape and the workpiece surface topography were coincident.

3 Influence of grinding process parameters on the *MRV* and *MRR*

Material removal has always been a big deal during the manufacturing process and the material removal rate has a direct connection with the period and cost of manufacturing. During the cutting process of randomly deflected truncated cone shape single abrasive grain, the grinding process parameters (wheel speed, wheel diameter, workpiece feed speed, cutting depth of the abrasive grain, δ_1 and δ_2) are very closely related to *MRV* and *MRR*, and play a very important role in the cutting process. Therefore, it is meaningful and important to analyse the *MRV* and *MRR* under different grinding parameters, discuss the rational selection and optimization of each

grinding process parameter in depth, and study the influence law of each parameter in the grinding process of single abrasive grain cutting in order to obtain higher grinding efficiency.

According to the previous subsection analysis, a Matlab calculation program was run under the parameters in Table 1, as shown in Fig.16.

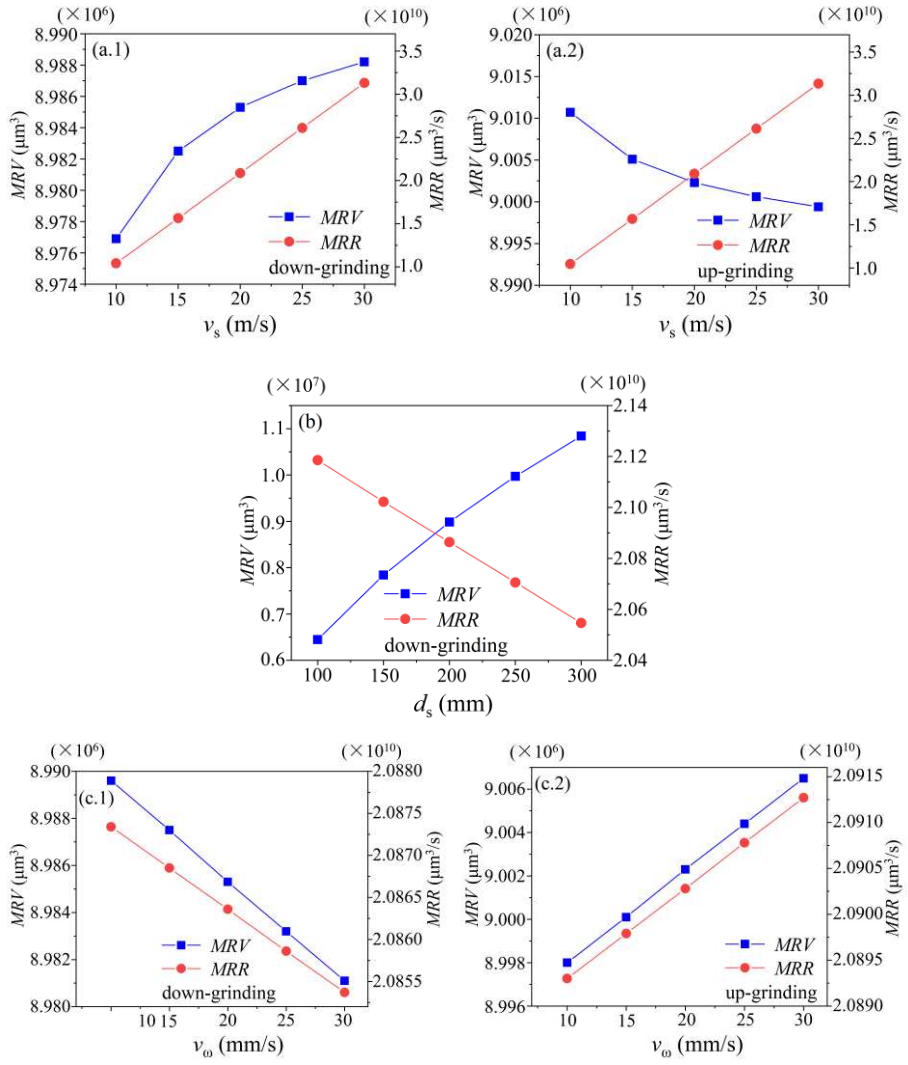

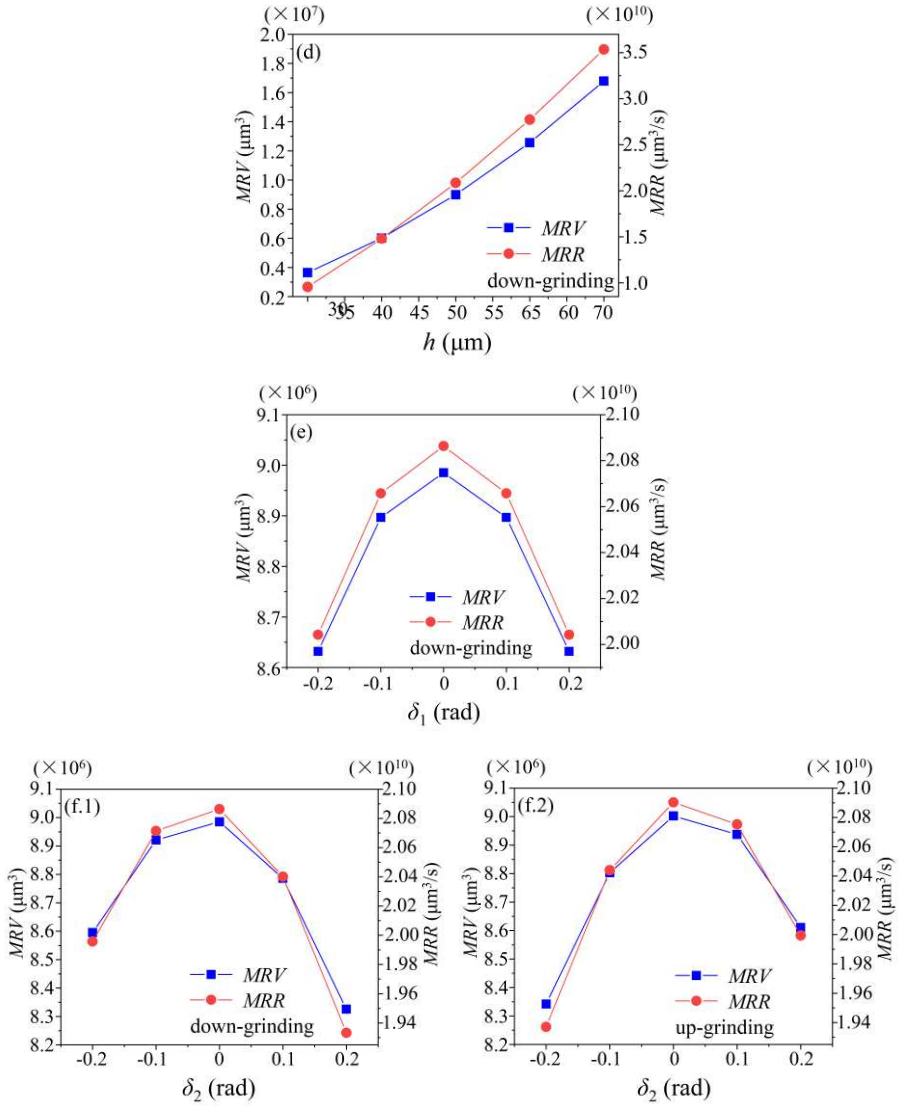

Fig.16. the values of *MRV* and *MRR* versus (a) wheel speed, (b) wheel diameter, (c) workpiece feed speed, (d) grain's cutting depth, (e) deflection angle δ_1, and (f) deflection angle δ_2.

As can be seen from Fig.16, the related results obtained were consistent with the findings in the relevant literature [25]. I.e., when the grinding method is down-grinding, the *MRV* decreases with the increment of the wheel speed; however, the *MRR* increases with the wheel speed. The *MRV* and *MRR* are increment with the increasing grain's cutting depth of abrasive grain. The *MRV* and *MRR* have increase with the workpiece feed speed.

The influence law of wheel diameter, Grain's cutting depth, and δ_1 during

up-grinding was similar to the down-grinding. Thus the calculated results were not described in this article, all conclusions are as follows:

(1) When the grinding method was down-grinding, the *MRV* increased with the increment of wheel speed, the growth rate decreased gradually, and the *MRR* also increased with the increment of wheel speed. When the grinding method was up-grinding, the changing way of *MRV* was the opposite of that in the down-grinding, while the *MRR* was the same. This indicated that a high wheel speed was able to enhance the *MRV*; however, when wheel speed increased to a certain value, its effect on *MRV* was not distinct. According to Eqs. (7) and (37), $\omega_s=v_s/r_s$, it can be seen that the *MRR* was both positively correlated with the wheel speed and the *MRV*, the variation range size of the *MRV* was not in the same order of magnitude as the variation range size of the wheel speed, which was negligible in comparison, so the *MRR* in the figure showed a linear increment with the increase of the wheel speed.

(2) The *MRV* increased with the growth of wheel diameter, the larger the wheel diameter the slower the change rate, based on the same reason as the first one, the *MRR* was both positively correlated with the wheel diameter and the *MRV*, thus, the *MRR* decreased linearly with the growth of wheel diameter. In addition, it was not affected by the pattern of the grinding method. So, increasing the grinding wheel diameter can increase the *MRV*, but it would decrease the *MRR*.

(3) When the grinding method was down-grinding, the *MRV* and *MRR* decreased with the increment of workpiece feed speed, and when the grinding method was up-grinding, the *MRV* and *MRR* increased with the increment of the workpiece feed

speed. Therefore, in the up-grinding condition, increasing the workpiece feed speed would help to improve the *MRR*.

(4) The *MRV* and *MRR* increased with the increment of the Grain's cutting depth, and the changing pattern was the same under different grinding methods. Therefore, increasing the Grain's cutting depth would help to improve the *MRR*, but the depth of the Grain's cutting cannot be increased indefinitely to avoid affecting the surface quality of the workpiece after cutting.

(5) For the deflection angle δ_1, regardless of the down-grinding or up-grinding, when the deflection angle δ_1 increased from small to large, the *MRV* and *MRR* increased first and then decreased, and there was a maximum value when the deflection angle was 0 rad. Thus, increasing the absolute value of the abrasive grain deflection angle δ_1, the *MRV* and *MRR* would be reduced.

(6) For the deflection angle δ_2, when the grinding method was down-grinding, the *MRV* and *MRR* increased first and then decreased with the deflection angle δ_2 increased from small to large, and the increase rate was less than the decrease rate. When the grinding method was down-grinding, and the deflection angle δ_2 increased from small to large, the *MRV* and *MRR* increased first and then decreased, however, the increase rate was larger than the decrease rate. This indicates that decreasing the absolute value of the deflection angle δ_2 could help to improve the *MRV* and *MRR*, and its change pattern was related to the grinding method.

4 Conclusion

In the present study, based on the random distribution characteristic of abrasive

grains on the grinding wheel circumference surface during the manufacturing process, in order to reflect the random distribution for the abrasive grains' position and angle, considering the grinding parameters and deflection parameters comprehensively, a theoretical model of cutting mechanism based on randomly deflected truncated cone shape single abrasive grain was established. The main contributions of this paper and the new findings are as follows.

Considering the grinding parameters and deflection parameters comprehensively, a mathematical case model of the moving motion trajectory of a randomly deflected truncated cone shape single abrasive grain was established. The trajectory length value calculated by the numerical method was verified, the obtained trajectory length error was extremely small between the numerical method and Malkin's formula, the maximum error less than 0.16%. The single abrasive grain of a randomly deflected truncated cone shape cutting process model was also established, the grain moving trajectory, ground surface topography and undeformed chip shape were obtained, and found that the undeformed chip shape and the workpiece surface topography were coincident for single grain cutting. The influence of the grinding parameters and deflection parameters on the *MRV* and *MRR* were studied. When the grinding method was up-grinding, the *MRV* decreases with the increasing wheel speed, while the *MRR* increases with wheel speed. The *MRV* increased with the growth of wheel diameter, while the *MRR* decreases with wheel diameter indicating that the high wheel speed and small wheel diameter are able to enhance the *MRR*. Both the *MRV* and *MRR* increase with the increment of cutting depth of abrasive grain or workpiece feed speed.

While the *MRV* and *MRR* decrease with the raising of absolute value of single abrasive grain deflection angle. The influence law on the *MRV* and *MRR* of down-grinding were similar or opposite trend to up-grinding. In summary, the basic theory of cutting mechanism based on randomly deflected truncated cone shape single abrasive grain was established. The obtained conclusions have great significance for the selection and optimization of grinding parameters, and the further study in the grinding mechanism of the grinding wheel.

Acknowledgements

The work was supported by the National Natural Science Foundation of China (Grant No. 51605240 and No. 51705272), National Science Foundation for Post-doctoral Scientists of China (Grant No. 2018M632643), and the Taishan Scholar Project of Shandong Province (Grant No. ts201511038).

Conflicts of interest/Competing interests: The authors declare no conflict of interest.

Availability of data and material: All data generated or analyzed during this study are included in this published article.

Authors' contributions: Conceptualization, Jingliang Jiang; methodology, Dexiang Wang and Shufeng Sun; investigation, Lansheng Zhang.; data curation, Lansheng Zhang; writing—original draft preparation, Lansheng Zhang; writing—review and editing, Dexiang Wang; supervision, Jingliang Jiang.

Code availability: Not applicable

Ethics approval: Not applicable

Consent to participate: Not applicable

Consent for publication: All authors have read and agreed to the published version of the manuscript.

Reference:

[1]Chen H, Zhao J, Wang Z, Dong J, Yu T (2021) Modeling virtual abrasive grain based on random ellipsoid tangent plane. Int J Adv Manuf Technol 113:2049–2064. https://doi.org/10.1007/s00170-021-06742-y

[2]Sun C, Hong Y, Xiu S, Yao Y, (2021) Grain refinement mechanism of metamorphic layers by abrasive grinding hardening. J Manuf Processes 69:125-141. https://doi.org/10.1016/j.jmapro.2021.07.040

[3]Agarwal S, Venkateswara Rao P (2010) Modeling and prediction of surface roughness in ceramic grinding. Int J Mach Tools Manuf 50:1065 – 1076. https://doi.org/10.1016/j.ijmachtools.2010.08.009

[4]Oliveira JFG, Silva EJ, Gomes JJF, Klocke F, Friedrich D (2005) Analysis of grinding strategies applied to crankshaft manufacturing. CIRP Ann - Manuf Technol 54:269–272. https://doi.org/10.1016/S0007-8506(07)60100-0

[5]Stephenson DJ, Sun X, Zervos C (2006) A study on ELID ultra precision grinding of optical glass with acoustic emission. Int J Mach Tools Manuf 46:1053–1063. https://doi.org/10.1016/j.ijmachtools.2005.08.013

[6]Caggiano A, Teti R (2013) CBN grinding performance improvement in aircraft engine components manufacture. Procedia CIRP 9:109–114.

https://doi.org/10.1016/j.procir.2013.06.177

[7]Dai C, Yu T, Ding W, Xu J, Yin Z, Li H (2019) Single diamond grain cutting-edges morphology effect on grinding mechanism of Inconel. Precision Engineering 55: 119-126.

https://doi.org/10.1016/j.precisioneng.2018.08.017

[8]Ren J, Hao M, Lv M, Wang S, Zhu B (2018) Molecular dynamics research on ultra-high-speed grinding mechanism of monocrystalline nickel. Appl Surf Sci 455:629-634.

https://doi.org/10.1016/j.apsusc.2018.06.042

[9]Anderson D, Warkentin A, Bauer R (2012) Comparison of spherical and truncated cone geometries for single abrasive-grain cutting. J Mater Process Tech 212(9):1946-1953.

https://doi.org/10.1016/j.jmatprotec.2012.04.021

[10]Gu P, Zhu C, Tao Z, Yu Y (2020) A grinding force prediction model for SiCp/Al composite based on single-abrasive-grain grinding.Int J Adv Manuf Technol 109:1563–1581.

https://doi.org/10.1007/s00170-020-05638-7

[11]Yin J, Xu J, Ding W, Su H (2012) Effects of grinding speed on the material removal mechanism in single grain grinding of SiCf/SiC ceramic matrix composite. Ceramics International 47(9):12795-12802.

https://doi.org/10.1016/j.ceramint.2021.01.140

[12]Malkin S (2008) Grinding technology: theory and application of machining with abrasives. Industrial Press Inc. New York

[13]Chen X, Rowe WB (2014) Analysis and simulation of the grinding process. Part I: generation of the grinding wheel surface. Eur Heart J 35:2264 – 2265.

https://doi.org/10.1093/eurheartj/ehu271

[14]Zhang Y, Li C, Ji H, Yang X, Yang M, Jia D, Zhang X, Li R, Wang J (2017) Analysis of grinding mechanics and improved predictive force model based on material-removal and plastic-stacking mechanisms. Int J Mach Tools Manuf 122:81–97.

https://doi.org/10.1016/j.ijmachtools.2017.06.002

[15]Aurich JC, Kirsch B (2012) Kinematic simulation of high-performance grinding for analysis of chip parameters of single grains. CIRP J Manuf Sci Technol 5:164–174.

https://doi.org/10.1016/j.cirpj.2012.07.004

[16]Bhushan B (2013) Introduction to tribology. Wiley

[17]Anandita S, Mote RG, Singh R (2017) Stochastic analysis of microgrinding tool topography and its role in surface generation. J Manuf Sci Eng Trans ASME 139:1–14.

https://doi.org/10.1115/1.4038056

[18]Koshy P, Jain VK, Lal GK (1997) Stochastic simulation approach to modelling diamond wheel topography. Int J Mach Tools Manuf 37:751–761.

https://doi.org/10.1016/S0890-6955(96)00086-7

[19]Wang S, Li C, Zhang D, Jia D, Zhang Y (2014) Modeling the operation of a common grinding wheel with nanoparticle jet flow minimal quantity lubrication. Int J Adv Manuf Technol 74:835–850.

https://doi.org/10.1007/s00170-014-6032-z

[20]Liu P, Lin B, Yan S, Li Y, Wang B (2016) Numerical simulation and experimental validation of fixed abrasive grinding pad topography. Int J Adv Manuf Technol 83:1253–1264.

https://doi.org/10.1007/s00170-015-7643-8

[21]Zhang X, Yao B, Feng W, Shen Z, Wang M (2015) Modeling of a virtual grinding wheel based on random distribution of multi-grains and simulation of machine-process interaction. J Zhejiang Univ Sci A 16:874–884.

https://doi.org/10.1631/jzus.A1400316

[22]Cooper WL, Lavine AS (2001) Grinding process size effect and kinematics numerical analysis. 122:59–69

[23]Wang X, Yu T, Dai Y, Shi Y, Wang W (2016) Kinematics modeling and simulating of grinding surface topography considering machining parameters and vibration characteristics. Int J Adv Manuf Technol 87:2459–2470.

https://doi.org/10.1007/s00170-016-8660-y

[24]Jiang J, Sun S, Wang D, Y Y, Liu X (2020) Surface texture formation mechanism based on the ultrasonic vibration-assisted grinding process. Int J Mach Tool Manuf 156:0890-6955.

https://doi.org/10.1016/j.ijmachtools.2020.103595

[25]Wang, C, Chen, J, Fang, Q, Liu F, Liu Y (2016) Study on brittle material removal in the grinding process utilizing theoretical analysis and numerical simulation. Int J Adv Manuf Technol 87:2603-2614.

https://doi.org/10.1007/s00170-016-8647-8